2015

Ferromagnetism in Laves-phase WFe_2 nanoparticles

Mark A. Koten
University of Nebraska-Lincoln, mkoten2@unl.edu

Priyanka Manchanda
University of Nebraska-Lincoln, priyanka.manchanda@vanderbilt.edu

Balamurugan Balamurugan
University of Nebraska-Lincoln, balamurugan@unl.edu

Ralph A. Skomski
University of Nebraska-Lincoln, rskomski2@unl.edu

David J. Sellmyer
University of Nebraska-Lincoln, dsellmyer@unl.edu

See next page for additional authors

Ferromagnetism in Laves-phase WFe_2 nanoparticles

M. A. Koten,[1] P. Manchanda,[2] B. Balamurugan,[2] R. Skomski,[2]
D. J. Sellmyer,[2] and J. E. Shield[1]
[1]*Department of Mechanical and Materials Engineering and Nebraska Center for Materials and Nanoscience, University of Nebraska, Lincoln, Nebraska 68588-0526, USA*
[2]*Department of Physics and Astronomy and Nebraska Center for Materials and Nanoscience, University of Nebraska, Lincoln, Nebraska 68588-0299, USA*

(Received 15 April 2015; accepted 29 June 2015; published online 9 July 2015)

While rare-earth based Laves phases are known to exhibit large magnetostriction, the magnetic properties of some binary Laves phases containing transition metals alone are not well known. This is because many of these compounds contain refractory elements that complicate melt processing due to high melting temperatures and extensive phase separation. Here, phase-pure WFe_2 nanoclusters, with the hexagonal C14 Laves structure, were deposited via inert gas condensation, allowing for the first known measurement of ferromagnetism in this phase, with M_S of 26.4 emu/g (346 emu/cm^3) and a K_U of 286 kerg/cm^3, at 10 K, and a T_C of 550 K. [http://dx.doi.org/10.1063/1.4926610]

For nearly a century, Laves phases[1] have been studied in a variety of scientific disciplines for different technological applications. Laves phases are dense-packed compounds of the type AB_2 that crystallize in one of three crystal structures: cubic C15, hexagonal C14, and hexagonal C36. They are known as size-factor-compounds because their formation is strongly dependent on the radius ratios of the A and B atoms;[2] the A atoms are coordinated by a large number of B atoms, and, in the hexagonal structures, the lattice constants follow the $c/a = 2\sqrt{2/3}$ relationship. In addition to exhibiting a variety of magnetic characteristics, some Laves phases are known superconductors,[3] while others have served as materials for metal-organic-frameworks[4] and rechargeable batteries.[5,6]

The RFe_2 Laves phase magnets, where "R" refers to the Lanthanide series, have the cubic C15 $MgCu_2$ type structure, large magnetic moments, and display large magnetostriction.[7] In the 1980s some investigations were made into TFe_2 Laves phases, where "T" represents another transition metal. Previous theoretical studies focused on predicting the type of magnetism that the Laves phases were likely to have based on their electronic structures.[8,9] However, this proved to be a challenge due to the complexities of transition metal magnetism.[10] Ishida *et al.*[9] used this method to predict the magnetism of the WFe_2 phase but their results were inconclusive. More recently, Kumar *et al.*[11] predicted that the C14-ordered phase is essentially ferromagnetic, with a small induced antiparallel or "ferrimagnetic" moment on the W site. Experimentally, the WFe_2 phase has been difficult to form and frequently been referred to as nonmagnetic.[12] However, the current thrust to find rare-earth-free permanent magnets with inexpensive components has renewed interest in TFe_2 compounds and other related structures.[11]

The equilibrium λ-WFe_2 Laves phase that forms in the C14 structure is a difficult bulk compound to produce due to slow diffusion kinetics and a nearly zero enthalpy of mixing.[13] As a result, there are no known reports in the literature detailing the phase-purity necessary to elucidate magnetic behavior.[2,12,14,15] The high melting point of W complicates melt processing, as does the large peritectic gap in the equilibrium phase diagram,[16] which creates extensive segregation during solidification that is difficult, if not impossible, to completely eliminate during homogenization heat treatment. Elemental Fe and W powders can be mechanically alloyed to the point of amorphization, though long milling times (about 300 h) lead to significant Fe contamination and uncertainty in the final composition.[17]

In this work, the magnetic and structural properties of WFe_2 nanoclusters are investigated experimentally and using density functional theory (DFT) calculations. WFe_2 nanoclusters were produced using a sputtering-based inert gas condensation (IGC) method. IGC is a powerful route to chemically homogeneous structures, as the clusters condense directly from the gas phase.[18–20] The compositions can be readily tailored, particularly if the gas source is sputtering, and both crystalline and amorphous structures have been observed.[20,21] As-deposited amorphous structures can be annealed to form equilibrium or near-equilibrium phases without affecting the composition.[22,23] Additionally, nanoscale ferromagnetism can differ from that of the bulk material because of a larger fraction of surface atoms with reduced nearest neighbors and uncompensated surface spins, which can lead to magnetization enhancement.[24] With this in mind, DFT calculations were performed for a 125 atom nanocluster for comparison to the aforementioned bulk calculation[11] and experimental results for clusters.

The condensation chamber was held between 17 and 21 °C by water cooling, and a mixture of Ar and He gases was flowed through the system in a ratio of 10:1 for an operating pressure of about 10^{-1} Torr. The nanoclusters were deposited at a power of 100 W on Si substrates for magnetic characterization and on Cu-mesh grids with an ultrathin C support film for transmission electron microscopy. To prevent particle agglomeration, oxidation, and inter-cluster diffusion, the Fe-W clusters were covered by a C film that was approximately 2 nm thick. Twenty-five layers of clusters were deposited onto the Si substrate, with each layer separated by the C layer, for magnetic measurements, and a single layer was deposited onto the Cu grids for electron microscopy. For post-deposition annealing, the sample was wrapped in Ta foil and placed inside a quartz tube and then sealed in an Ar atmosphere prior to annealing at 600 °C for 30 min. The furnace was then switched off and the samples remained inside until the furnace temperature returned to room temperature.

The sputtering target (7.62 cm in diameter) was made by embedding six 99.95% pure W plugs (6.35 mm in diameter) in the expected etching region ("racetrack") of a Fe disk. The area of the etching region and the sputtering yields for Fe and W factored into the placement and number of plugs embedded in the target for an expected composition of 67 at. % Fe. The composition was determined by energy dispersive x-ray spectroscopy (EDS) using an FEI Tecnai Osiris scanning transmission electron microscope (S/TEM) operating at 200 kV on regions containing both isolated, single clusters and thousands of clusters. The particle size distributions were determined from bright-field TEM images sampling approximately 800 clusters, and then quantified using the ImageJ software.[25] The crystal structure was determined by selected area diffraction (SAD) patterns and fast Fourier transforms (FFTs) of high-resolution TEM images. Magnetic hysteresis was measured at 10 and 300 K after annealing using a Quantum Design Magnetic Property Measurement System (MPMS) superconducting quantum interference device (SQUID) magnetometer. The Curie temperature was found by measuring magnetic moment between 300 and 850 K on a Quantum Design Physical Properties Measurement System (PPMS). The diamagnetic signal from the Si substrate was subtracted from the hysteresis loops. The law of approach to saturation method[26] was used to calculate the anisotropy constant for the WFe_2 clusters, and the saturation magnetization was found by fitting a line to a plot of the high field M vs $1/H^2$ data.

The DFT calculations were carried out using the projected augmented wave (PAW) method, as implemented in the Vienna *ab initio* simulation package (VASP).[27,28] The exchange-correlation effects described by Perdew, Burke, and Ernzerhof (PBE) were implemented by the generalized-gradient approximation (GGA).[29] The optimized lattice parameters ($a = 4.735$ Å, $c = 7.732$ Å) were used, which are in good agreement with the experimental lattice parameters. A supercell with 15 Å vacuum spaces along x, y, and z was used to ensure that there was no interaction between neighboring WFe_2 nanoclusters. For the nanocluster, the Γ-point was used for k-point sampling due to the large supercell. The atomic positions for the clusters were relaxed until the force acting on each atom was less than 0.1 eV/Å, and a convergence criterion of 1×10^{-5} eV has been used for electronic structure calculations.

The composition was determined by EDS in both the as-deposited and annealed clusters using both regions that encompassed many nanoparticles and from single nanoparticles. The composition was found to be between 67 and 68 at. % Fe, which is within the error of the EDS quantification

software. The overall uniformity of the cluster composition was excellent, which led to the fabrication of a phase-pure sample. This has been a challenge using other processing techniques for this system and specifically for the WFe_2 phase.

The TEM images of the as-deposited clusters revealed some clusters to have formed in the WFe_2 structure while others were poorly crystalline or even amorphous. In general, the amount of crystallinity increased with particle size. In Fig. 1(a) the high resolution TEM image of a 15 nm particle is indexed to the [0001] zone axis of the λ-WFe_2 hexagonal crystal structure with lattice constants a = 4.64 ± 0.09 and c = 7.57 ± 0.14 Å (Fig. 1(b)). The lattice fringes extending across the entire nanoparticle indicate that it is a single crystalline WFe_2. The lattice parameters are in agreement with the values reported in Pearson's handbook.[30] The size distribution data (Fig. 1(c)) were compiled from several images, and then analyzed by fitting the data to a Gaussian function. From this analysis, the mean cluster size was determined to be 5.0 ± 2.5 nm. The reflections in the SAD pattern were also indexed to the C14 structure, although there were very few reflections to index. Considering the large number of nanoparticles sampled, the few reflections observed are further evidence that the nanoparticles may not be all crystalline. Since the WFe_2 structure is the equilibrium structure at this composition, the nanoclusters were annealed to induce formation of the WFe_2 phase.

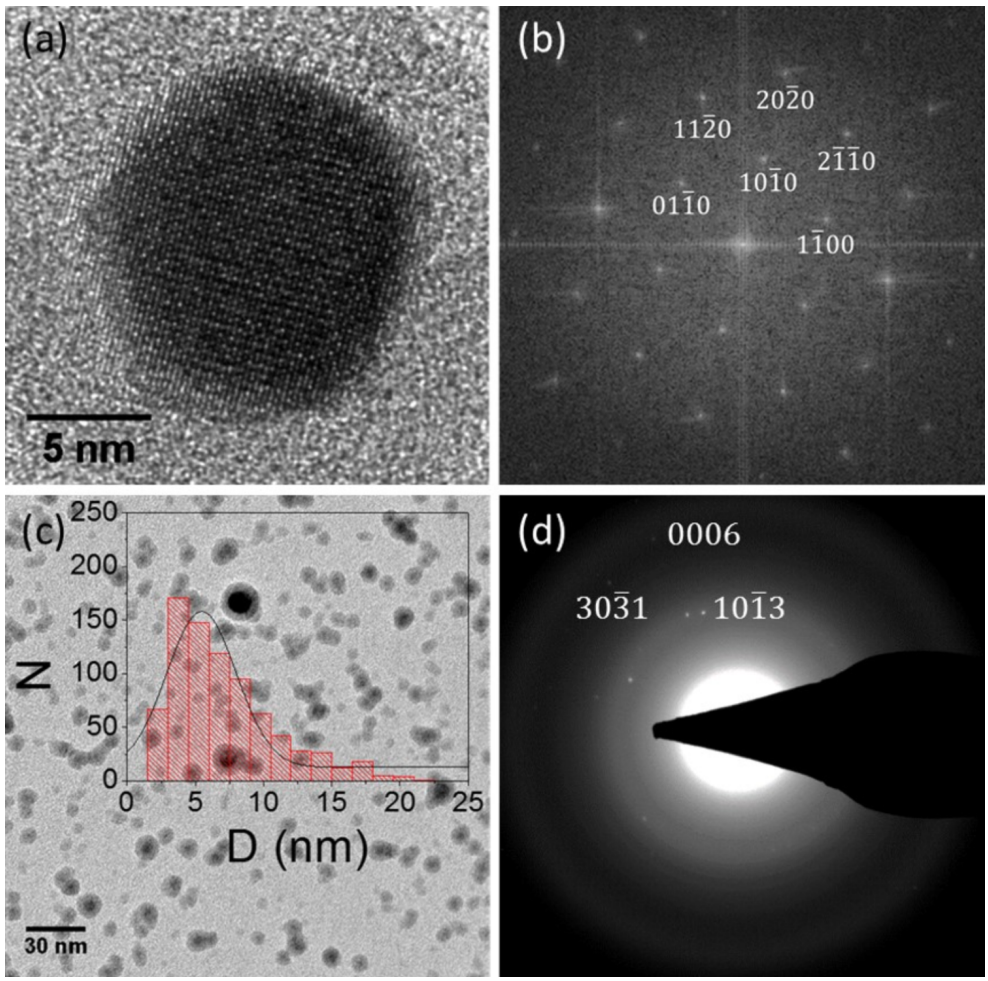

FIG. 1. (a) High resolution TEM micrograph of an as-deposited nanocluster with (b) corresponding FFT indexed to the [0001] zone axis of the Laves phase. (c) TEM micrograph with inset size distribution histogram. (d) SAD pattern with a few spots indexed to the WFe_2 structure.

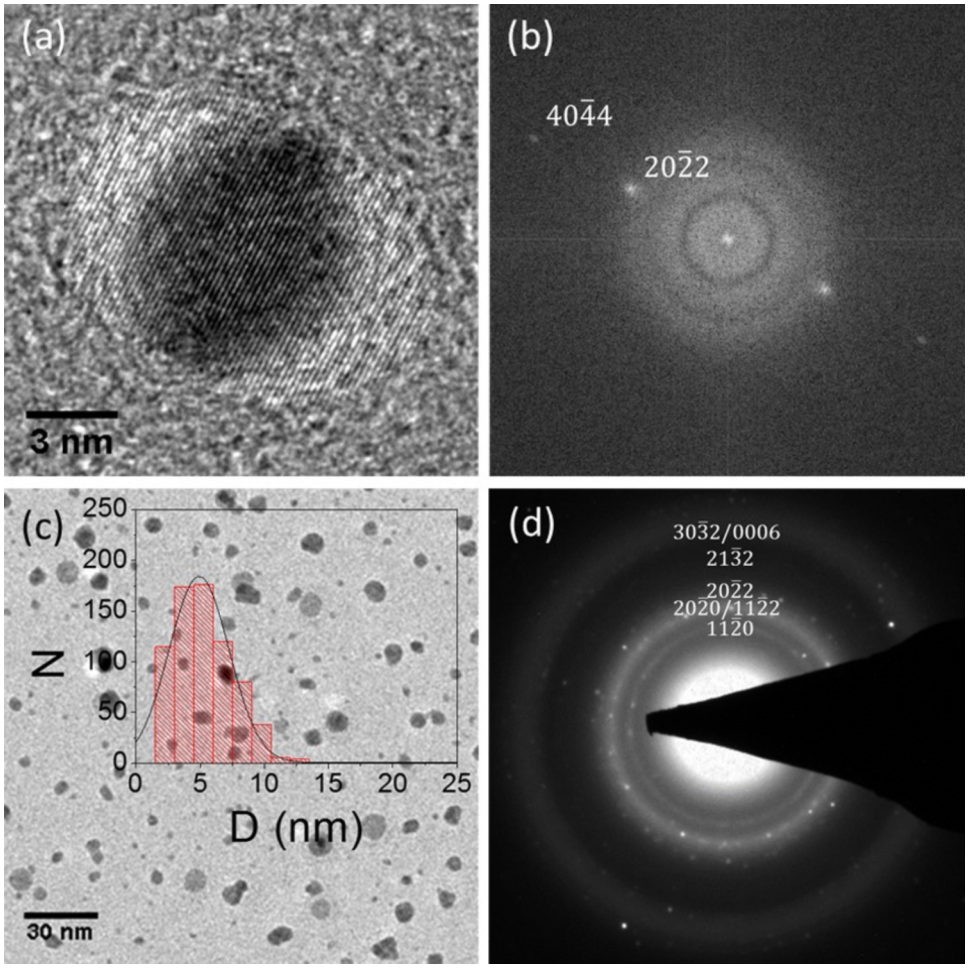

FIG. 2. (a) A high resolution image of an annealed WFe_2 cluster with (b) the indexed FFT. (c) A low magnification TEM image displaying the post annealing morphology and particle size distribution (inset). (d) A SAD pattern indexed to the WFe_2 structure.

Fig. 2 shows the structure and morphology of the clusters after annealing. The high resolution image and FFT of an 8 nm particle show that the nanoparticle is single crystalline, while the SAD pattern (Fig. 2(d)) shows strong and sharp diffraction maxima indicating that the crystal quality has improved with annealing. The increase in the number of spots in the SAD pattern compared to the as-deposited image is evidence that all or most of the clusters are crystalline WFe_2. Additionally, the lattice parameters were calculated again from the SAD pattern and were in agreement with the as-deposited structure and are closer to the accepted values for the WFe_2 phase ($a = 4.72 \pm 0.10$ Å, $c = 7.71 \pm 0.16$ Å). Some large agglomerations did form during annealing (not shown) where several particles effectively sintered into large particles, sometimes as large as 50 nm. However, this occurred very infrequently and did not markedly affect the size distribution data or Gaussian fit. The size distribution shown in Fig. 2(c) for the annealed clusters showed that the particle size and morphology changes after annealing were negligible, and the average size remained 5.0 nm. Thus, after annealing, IGC has successfully produced the WFe_2 Laves phase with the phase-purity necessary to elucidate the magnetic properties.

Earlier reports suggest that the λ-WFe_2 phase is paramagnetic,[12] although recent first-principle calculations indicate that this structure is ferrimagnetic with the small W moments aligning anti-parallel to those of Fe. Figure 3(a) shows the WFe_2 nanocluster that was created for the DFT calculations. The calculated average magnetic moment is 1.65 μ_B per Fe atom (58 emu/g) for the nanocluster. This value is high compared to 0.92 μ_B per Fe atom (33.8 emu/g) reported for bulk

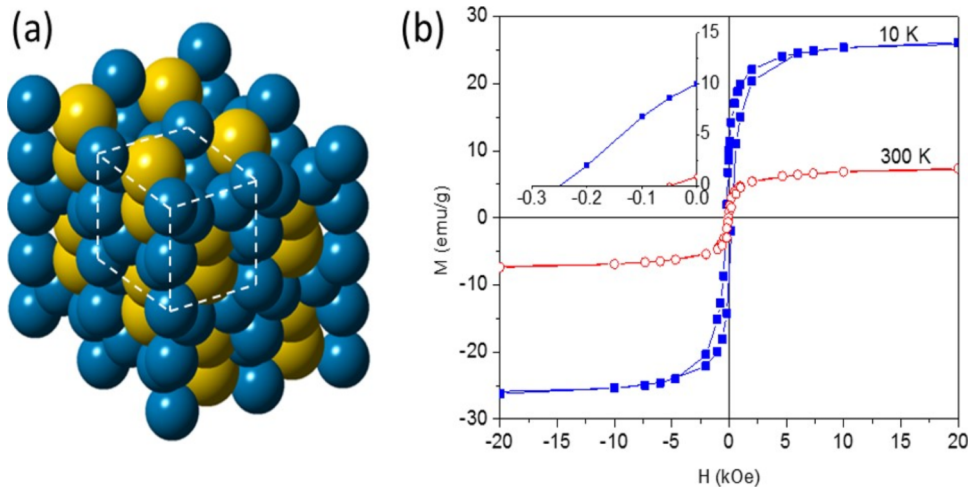

FIG. 3. (a) Schematic of a 1.8 nm WFe_2 nanocluster used in the DFT calculations. Blue and yellow spheres represent the Fe and W atoms, respectively. (b) Hysteresis loops measured at 10 and 300 K for the WFe_2 nanoclusters. The inset shows details of the second quadrant.

WFe_2.[11] The enhancement in the magnetic moment at the nanoscale arises from increased moments of Fe atoms at the surfaces. These surface Fe atoms have magnetic moments of about 2.5 μ_B, larger than the Fe magnetic moments in bcc α-Fe, whereas Fe atoms near the core have moments of about 0.8 μ_B. In any case, the W moment is very low relative to Fe at -0.21 μ_B. For this geometry, the ratio of the number of surface atoms N_S to the number of volume atoms N_V is larger than 5, and the total number of atoms included is 125. For a spherical 1.5 nm cluster containing 117 atoms, the ratio $N_S/N_V = 2.3$, which means that the number of surface atoms is strongly affected by not only the size but also the chosen geometry. Therefore, enhancements in the magnetization due to surface contributions may play a role in these nanostructures. The experimental investigations were also aimed at determining if such enhancements in magnetic moments would be observed in the size range here, i.e., 5 nm in diameter.

The magnetic properties of the nanoclusters were determined from hysteresis loop measurements (Fig. 3(b)) obtained at 10 and 300 K. The inset shows second quadrant behavior. The coercivity at 10 K was 250 Oe and decreased to 50 Oe at 300 K. Similarly, the remanence decreased from 10 emu/g to 1 emu/g over the same interval. The saturation magnetization was found to be 26.4 ± 0.1 emu/g at 10 K and 7.3 ± 0.1 emu/g at 300 K, and the anisotropy constants K_1 were 286 and 92 kerg/cm^3 at 10 K and 300 K, respectively. The magnetization is on the order of the predicted bulk saturation magnetization of the WFe_2 phase (33.8 emu/g). A Curie temperature of 550 K was also measured from a temperature sweep of magnetic moment (not shown). Thus, no enhancement in the magnetic properties arising from the predicted larger magnetic moments of the surface atoms was observed. The particle sizes are likely too large for surface effects to significantly enhance the magnetization, as the fraction of surface atoms is too low. For a 2.5 nm diameter nanoparticle, the surface atom-to-volume atom ratio $N_S/N_V = 1$. From the annealed size distribution (Fig. 2(c)), only a small fraction of the nanoparticles is below this critical size, where the number of surface atoms exceeds the number of volume atoms.[31] Surface atoms here are defined as atoms positioned within 2.5 Å of the cluster surface. Further, the DFT calculations of the nanocluster may overestimate the overall magnetization due to the shape of the model 125 atom nanocluster (1.8 nm with high aspect ratio), as there is a larger number of surface atoms with respect to a more spherical geometry. Additionally, the magnetization measured here is about 80% of the predicted bulk saturation, which has been reported before. The M_S of Co clusters embedded in a SiO_2 matrix were on the order of 75% to 85% of the bulk value, which is consistent with the reductions observed here for WFe_2 embedded in C.[32]

In summary, the WFe_2 Laves phase has been successfully formed via inert gas condensation, and SQUID magnetometry has shown that this phase is ferromagnetic. Formation of this phase was

a significant experimental challenge, but characterization of these nanoparticles revealed that they had a high degree of phase purity. While some of the larger as-deposited clusters formed in the Laves phase, the majority of the clusters showed traces of amorphous, poorly crystalline structure. Heat treatment resulted in the formation of the equilibrium phase in nanoparticles with an average size of 5 nm. The WFe_2 phase is ferromagnetic up to about 550 K. At 10 K, the saturation magnetization is 26.4 ± 0.1 emu/g, the coercivity is 250 Oe, and the anisotropy constant was determined to be 286 kerg/cm^3. The experimental results show that the cluster's magnetization is closer to the bulk calculations because the particle sizes were not small enough to observe an increase in magnetization due to surface effects. The low coercivity for a hexagonal structure is likely a consequence of the low anisotropy constant, which is explained by the WFe_2 phase having easy-plane anisotropy along the ⟨1000⟩ directions rather than easy-axis anisotropy in the [0001] direction.

J.E.S and M.A.K were financially supported by the U.S. NSF-MPS-DMR (Grant No. 0820521, Program Director D. Finotello). D.J.S, R.S, P.M, and B.B were supported by the U.S. DOE BES (Grant No. DE-FG02-04ER46152, Program Director M. Pechan). Research was performed in the facilities of the Nebraska Center for Materials and Nanoscience, which are supported by the Nebraska Research Initiative.

[1] F. Laves and H. Witte, Metallwirtsch **14**, 645 (1935).
[2] A. K. Sinha and W. Hume-Rothery, J. Iron Steel Inst. **205**, 1145 (1967).
[3] C. Pfleiderer, M. Uhlarz, S. M. Hayden, R. Vollmer, H. V. Lohneysen, N. R. Bernhoeft, and G. G. Lonzarich, Nature **412**, 58 (2001).
[4] S. Hong and C. L. Fu, Phys. Rev. B **66**, 094109 (2002).
[5] K. Young, M. A. Fetcenko, F. Li, and T. Ouchi, J. Alloys Compd. **464**, 238 (2008).
[6] H. Nakano, S. Wakao, and T. Shimizu, J. Alloys Compd. **253-254**, 609 (1997).
[7] K. H. J. Buschow, Rep. Prog. Phys. **40**, 1179 (1977).
[8] S. Ishida, S. Asano, and J. Ishida, J. Phys. Soc. Jpn. **54**, 3925 (1985).
[9] S. Ishida, S. Asano, and J. Ishida, J. Phys. Soc. Jpn. **54**, 4695 (1985).
[10] S. Asano and S. Ishida, J. Phys. F: Met. Phys. **18**, 501 (1988).
[11] P. Kumar, A. Kashyap, B. Balamurugan, J. E. Shield, D. J. Sellmyer, and R. Skomski, J. Phys.: Condens. Matter **26**, 064209 (2014).
[12] A. A. Novakova, V. V. Lyovina, D. V. Kuznetsov, and A. L. Dzidziguri, J. Alloys Compd. **318**, 423 (2001).
[13] G. H. Lee, S. H. Huh, J. W. Park, and H. K. Kim, J. Phys. Chem. B **105**, 5856 (2001).
[14] U. Herr and K. Samwer, Nanostruct. Mater. **1**, 515 (1992).
[15] K. Sumiyama, M. Hirata, and W. Teshima, Jpn. J. Appl. Phys. **30**, 2839 (1991).
[16] T. B. Massalski, H. Okamoto, P. R. Subramanian, and L. Kacprzak, in *Binary Alloy Phase Diagrams*, 2nd ed. (ASM International, 1990), Vol. 2.
[17] M. A. Koten and J. E. Shield, "Mechanical alloying within the Fe-W and Fe-Ta systems" (unpublished).
[18] H. Haberland, M. Karrais, M. Mall, and Y. Thurner, J. Vac. Sci. Technol. A **10**, 3266 (1992).
[19] S. H. Baker, S. C. Thornton, K. W. Edmonds, M. J. Maher, C. Norris, and C. Binns, Rev. Sci. Instrum. **71**, 3178 (2000).
[20] B. Balasubramanian, R. Skomski, X. Li, S. R. Valloppilly, J. E. Shield, G. C. Hadjipanayis, and D. J. Sellmyer, Nano Lett. **11**, 1747 (2011).
[21] F. Golkar, M. J. Kramer, Y. Zhang, R. Skomski, D. J. Sellmyer, and J. E. Shield, J. Nanopart. Res. **15**, 1638 (2013).
[22] P. Mukherjee, Y. Zhang, M. J. Kramer, L. H. Lewis, and J. E. Shield, Appl. Phys. Lett. **100**, 211911 (2012).
[23] E. Folcke, R. Lardé, J. M. L. Breton, M. Gruber, F. Vurpillot, J. E. Shield, X. Rui, and M. M. Patterson, J. Alloys Compd. **517**, 40 (2012).
[24] O. Šipr, M. Košuth, and H. Ebert, Phys. Rev. B **70**, 174423 (2004).
[25] C. A. Schneider, W. S. Rasband, and K. W. Eliceiri, Nat. Methods **9**, 671 (2012).
[26] G. Hadjipanayis, D. J. Sellmyer, and B. Brandt, Phys. Rev. B **23**, 3349 (1981).
[27] G. Kresse and J. Furthmüller, Comput. Mater. Sci. **6**, 15 (1996).
[28] G. Kresse and D. Joubert, Phys. Rev. B **59**, 1758 (1999).
[29] J. P. Perdew, K. Burke, and M. Ernzerhof, Phys. Rev. Lett. **77**, 3865 (1996).
[30] P. Villars, in *Pearson's Handbook Desk Edition Crystallographic Data for Intermetallic Phases* (ASM International, 1997), Vol. 2.
[31] F. Bodker, S. Morup, and S. Linderoth, Phys. Rev. Lett. **72**, 282 (1994).
[32] Y. Qiang, R. F. Sabiryanov, S. S. Jaswal, Y. Liu, H. Haberland, and D. J. Sellmyer, Phys. Rev. B **66**, 064404 (2002).